Structure−Property Relationships in the Nonlinear Optical Crystal $KTiOPO_4$ Investigated Using NMR and ab Initio DFT Calculations

P. A. Thomas,* A. Baldwin, and R. Dupree

Department of Physics, University of Warwick, Coventry CV4 7AL, U.K.

P. Blaha and K. Schwarz

Institute of Materials Chemistry, Vienna University of Technology, A-1060 Vienna, Getreidemarkt 9/165-TC, Austria

A. Samoson

National Institute for Chemical Physics and Biophysics, Akadeemia Tee 23, Tallinn, Estonia

Z. H. Gan

Center for Interdisciplinary Magnetic Resonance, National High Magnetic Field Laboratory, 1800 East Paul Dirac Drive, Tallahassee, Florida 32310

Received: November 13, 2003; In Final Form: January 29, 2004

^{17}O, ^{39}K, and $^{47,49}Ti$ solid-state NMR studies of the nonlinear optical crystal potassium titanyl phosphate, $KTiOPO_4$ (KTP), are reported. The results are compared with ab initio calculations using the WIEN2k program and discussed in specific relation to the bond-polarizability approach for the calculation of second-order nonlinear optical properties. It is found that the oxygen atoms in the anomalously short bonds to the titanium atoms (denoted by OT) have a considerably more ionic environment than the oxygen atoms (denoted by OP) that are involved in bridging TiO_6 octahedra and PO_4 tetrahedra. This result is consistent with the fractional covalencies computed using bond-polarizability principles for the Ti−OT and Ti−OP bonds, respectively. The NMR experiments are shown to validate independently the bond-polarizability approach to the calculation of nonlinear activity in KTP and demonstrate conclusively that the original notion that strong covalency in the short Ti−OT bonds is the principal source of nonlinear activity is incorrect. The field gradients at the Ti sites are estimated from NMR experiments to be ∼40 MHz, in agreement with WIEN2k calculations. These values are much larger than any found in previous studies of titanates and cannot be explained by models based on the distortion of the local octahedral oxygen coordination environment. It is suggested that both the large field gradient at the Ti sites and the variation of characteristics displayed by the different oxygen atoms in the structure may arise from other significant interactions, such as delocalization of charge or charge transfer, in significant structural chains of polyhedral units.

1. Introduction

Potassium titanyl phosphate, $KTiOPO_4$ (KTP), is well-known as a nonlinear optical crystal for frequency conversion.[1] In the last fifteen years, numerous isostructural compositional analogues of KTP, of general formula type M^ITiOXO_4 (where X is most commonly P or As) have been synthesized and studied (see, for example refs 2 and 3 for listings). Sometimes, these studies have been motivated by the desire to improve upon the combination of physical properties displayed by KTP, but more often the aim has been to determine the structural origin of the high optical nonlinearity by comparison of KTP with its structural analogues. Initial investigations[4,5] of the structural origin of the optical nonlinearity in KTP focused on the two types of highly distorted TiO_6 octahedra in the structure (Figure 1), each of which displays one anomalously short Ti−O bond (of length <1.74 Å). Within the bond-polarizability model of Levine,[6] these bonds are assigned a high polarizability because of both their short length and their presumed highly covalent nature compared with the other Ti−O bonds of more usual lengths (1.9−2.1 Å). When the contributions of the different bonds in the structure are added together tensorially to compute the nonlinear optical response, the short Ti−O bonds are weighted more highly than any others, leading to the conclusion that the presence of highly distorted TiO_6 octahedra is the key requirement for a high nonlinear optical (NLO) response. This interpretation was lent credence by early charge density studies,[7] which indicated an excess of electron density in the Ti−O short bonds, consistent with covalent character and high bond polarizability. Subsequent work on $NaTiOPO_4$[8] threw doubt on this point of view since the TiO_6 octahedra are at least as distorted as those in KTP yet the NLO response (measured by powder second-harmonic generation) is reduced by a factor of 10. Substitution of K by Li on one of the two independent sites (the K2 site) of the KTP structure was also observed to produce a decrease in the optical nonlinearity in the presence of high octahedral distortions.[9] It has also been demonstrated that the optical nonlinearity of $KTiOAsO_4$ is larger than that of KTP despite very similar octahedral distortions. This was principally

10.1021/jp037473n CCC: $27.50
Published on Web 03/16/2004

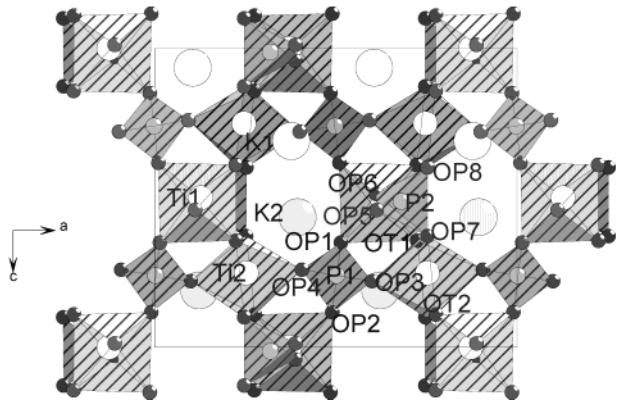

Figure 1. View of the crystal structure of KTP along the [010] direction. Ti1 and Ti2 are shown as white circles within light gray octahedra. P1 and P2 are shown as light gray circles within medium gray tetrahedra. K1 and K2 are shown as large white circles in the cages enclosed by the framework. Oxygens OT1, OT2, and OP1−OP8 are indicated by small dark circles at the corners of the coordination polyhedra. The structural coordinates were taken from ref 7, but the atoms have been renamed so that OP1−OP4 are bonded to P1 and OP5−OP8 are bonded to P2, with OT1 and OT2 making short bonds to Ti2 and Ti1, respectively. The sense of the $+c$ axis shown by the axes is opposite to the sense of the ferroelectric polarization ($\mathbf{P}_s$) for the structure as drawn.

accounted for by the increase in the linear optical susceptibilities brought about by the substitution of P by the more highly polarizable species As.[10] However, in a more recent paper containing updated bond-polarizability calculations,[11] it has been claimed that the principal source of the optical nonlinearities in both KTP and KTA is the $P2O_4$ ($As2O_4$) tetrahedron and the $K1O_8$ and $K2O_9$ groups rather than the TiO_6 groups. Recent charge density studies[12] of the KTP isomorph $RbTiOAsO_4$ have shown that electron density is not preferentially located in the short Ti−O bonds, as first suggested by Hansen et al.[4] for KTP, but in the longest and intermediate-length bonds of the TiO_6 octahedra.

Against this background, it remains of current interest to undertake investigations of KTP with a view to developing an understanding of the origin of the optical nonlinearity. Although numerous crystallographic studies of the average structure have been undertaken, investigations of the local structure, particularly that of the Ti and its associated oxygen coordination environment, have been few. Thus far, NMR investigations have been confined to the P sites[13−15] and the M^I sites when substituted with Na.[15] In this paper, we report an extensive experimental study using ^{39}K, ^{17}O, and $^{47,49}Ti$ NMR of the bonding environments and electric field gradients at these important atomic sites in KTP together with the results of ab initio DFT calculations using the WIEN2k code.[19] Ti NMR investigations are relatively unusual but have been shown to be both feasible and valuable, for example, in a wide-ranging study of TiO_6 octahedral compounds of the perovskite and ilmenite families, in which a systematic linear relationship between the measured electric field gradient at the Ti site and the distortion of the TiO_6 environment was determined.[16] In the perovskite family, the structure is formed by close-packed corner-sharing BO_6 octahedra with cube-octahedral sites being enclosed for the accommodation of the A cation in the ABO_3 formula type. In KTP, however, the major structural features are chains of corner-linked TiO_6−PO_4 octahedra and tetrahedra running along the [100] and [010] directions, with spiralling chains of corner-linked TiO_6 octahedra cross-threading the structure along the [011] and [01−1] directions. As a logical extension of the previous work it is of interest to determine whether the characteristics of the octahedral Ti environment in KTP are similar to those for the perovskite and ilmenite structures and to what extent KTP can be considered as an oxygen-octahedral ferroelectric given the additional complexities of its crystal structure.

2. Experimental Details

2.1. Synthesis of KTP Samples. The KTP samples for the ^{17}O NMR experiments were prepared from isotopically enriched TiO_2. The ^{17}O enrichment was achieved by first preparing the required amount of titania via a sol−gel route, which entailed the hydrolysis of titanium isopropoxide using 40% ^{17}O-enriched water. The sol−gel product was pumped on for several hours in order to produce a fine white powder, heat treated at approximately 110 °C for 4 h, and then washed with deionized water to remove any remaining organic contaminants from the hydrolysis reaction. The enriched TiO_2 was then used in a solid-state reaction to produce KTP according to the equation

$$KH_2PO_4 + TiO_2 \rightarrow KTiOPO_4 + H_2O \qquad (1)$$

The calcination of the starting materials was performed in a sealed quartz tube, which was first evacuated and then repressurized with ^{17}O-enriched O_2 gas to approximately half an atmosphere. The reagents were then heated to 700 °C for 8 h and were slowly cooled to room temperature. This procedure yielded a small amount (∼0.5 g) of enriched material. The powder was found to be composed principally of KTP with a small (estimated by XRD to be <10%) impurity phase, which was identified as anatase (TiO_2). Samples for ^{39}K NMR and single crystals for $^{47,49}Ti$ NMR were obtained from commercial suppliers.

2.2. NMR Experiments. The ^{39}K NMR work was performed on a CMX600 infinity spectrometer using a 9 mm CMX magic angle spinning (MAS) probe. An echo pulse sequence ($\tau-t-2\tau$) with whole echo acquisition was used because of long spectrometer deadtimes associated with the low-frequency operation and ringing effects generated by the piezoelectric nature of the KTP sample. The pulse length τ was 3 μs with an echo delay t of 200 μs, a recycle time of 1 s, and 67 500 acquisitions. The spectra were referenced to the secondary standard of solid KBr at 0 ppm.

The ^{17}O magic angle spinning experiments were performed on CMX infinity spectrometers at field strengths of 5.6, 8.45, and 14.1 T. CMX 3.2 and 4 mm MAS probes were used with the high-field spectrometer, and a Bruker 4 mm probe was used at the lower fields with typical spinning speeds of ∼12 kHz. All spectra were referenced to the primary standard of H_2O at 0 ppm.

Because two types of O sites are present in KTP, one with a low value of C_q (∼1 MHz) and the other with a much larger value (∼5 MHz), different data collection parameters were used to examine the different sites. For the high C_q sites, rotor-synchronized Oldfield echo sequences were used with solid $\pi/2$ and π pulses and recycle times of 1 s. For the low C_q sites, one-pulse experiments were used with recycle times of 4 s and a solids $\pi/2$ pulse length.

^{17}O measurements of KTP were also performed using the double-rotation (DOR) technique in order to improve the spectral resolution in the 200 to 0 ppm shift region where the eight quadrupolar-broadened lines from the OPs overlap. Spectra were obtained at the outer rotor speeds of 1300 and 1400 Hz at each of the field strengths of 11.7 and 16.95 T. A sideband suppression acquisition sequence program was used to halve

the number of sidebands appearing thus greatly increasing the clarity of the spectrum.

^{47,49}Ti measurements were attempted on a single-crystal sample. However, the combination of two distinct Ti sites, each with two Ti isotopes of similar gyromagnetic ratio but different quadrupole moments, on general positions of multiplicity four in the unit cell causes the spectrum to be complex from the outset. Furthermore, in KTP, the Ti lines were discovered to cover a very wide frequency range and to be extremely sensitive to the angle of the crystal, meaning that it was not feasible to collect rotation patterns in the usual way. NMR data for the Ti sites were finally taken from a powder sample using a CMX 9 mm MAS probe, which was operated without spinning. The spectra were acquired with an echo sequence (1.8 μs−80 μs−3.6 μs, a recycle delay of 1 s). The spectral width of the line precluded observation within a single experiment. The response was recorded in 80 kHz steps with 23 500 acquisitions per step, retuning the probe on each step until no signal was observed on either side of the initial frequency. The final line shape was constructed from the sum of these separate measurements.

3. WIEN2k Calculations

The theoretical calculations are based on density functional theory (DFT) and, more specifically, the use of the generalized gradient approximation (GGA) of Perdew et al.[17] The full potential (linearized) augmented plane wave + local orbitals (L/APW+lo) method[18] was utilized, as implemented in the WIEN2k code.[19] In this method, the unit cell is partitioned into spheres centered on the atomic sites and an interstitial region. In the latter, plane waves are used as basis functions, whereas in the former, an atomic-like expansion into numerical radial functions times spherical harmonics (up to $l = 10$) is used. Each partial wave is matched in value at the sphere boundary to the corresponding plane wave with a coefficient $A_{lm}(\mathbf{k_n})$. The radial functions are solutions of the radial Schrödinger equation for given angular momentum and fixed energy, E_l. The necessary flexibility of the basis is gained by additional "local orbitals" (lo), which consist of a linear combination of the same radial function and its energy derivative. They are not matched to any plane wave but are constrained to have zero value at the sphere boundary.

Sphere sizes of 2.0, 1.8, 1.55, and 1.3 bohr for K, Ti, P, and O spheres, respectively, were used. A basis of about 8500 plane waves (corresponding to $R_{\min}K_{\max} = 5.6$) was used, and the Brillouin zone (BZ) integration was done with 12 k-points in the irreducible BZ. The crystal structural data of Delarue et al.[20] were taken as input for the theoretical calculations.

The full electric field gradient (EFG) tensor was calculated from the total self-consistent charge density $\rho(r)$ in the crystal without further approximations. For example, the principal EFG component, V_{zz}, was obtained using

$$V_{zz} \approx \int \frac{\rho(r) Y_{20}(\hat{r})}{r^3} \, \mathrm{d}\vec{r} \qquad (2)$$

where Y_{20} is a spherical harmonic with $l = 2$ and $m = 0$. Because all electrons are taken into account, the charge redistribution is automatically achieved in the self-consistent field procedure, and thus no additional Sternheimer (anti) shielding factors are needed to explain the EFG. This method has been successfully applied to many types of solids[21−23] and has usually led to an agreement within 10−20% with the experimental values.

4. Experimental Results

^{39}K, ^{17}O MAS, and ^{17}O DOR spectra are shown in Figures 2−4, respectively. The static ^{39}K spectra (Figure 2) can be closely simulated by the sum of two quadrupolar line shapes, which have approximately the same integrated signal intensity, in agreement with two distinct K sites, K1 and K2, of equal occupancy. The fitting parameters are the quadrupolar coupling coefficient, $C_q = eQV_{zz}/h$ (MHz), where Q is the nuclear quadrupole moment taken from the theoretical calculations from Pyykkö,[24] V_{zz} is the principal component of the EFG, and η is the asymmetry parameter. These are listed in Table 1 together with the results of the WIEN2k calculations.

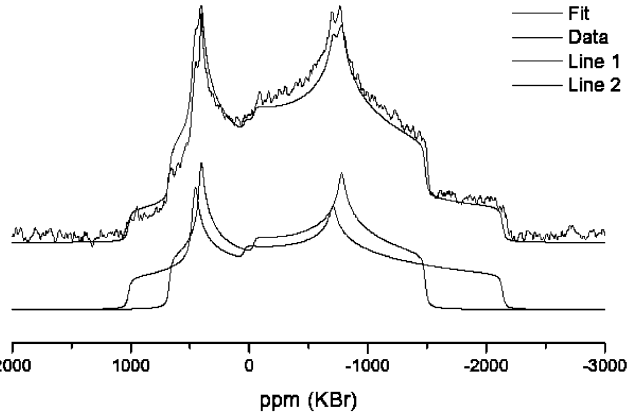

Figure 2. ^{39}K static NMR spectrum and line shape simulation for the K1 and K2 sites in KTP.

The ^{17}O spectra collected at the three different field strengths consist of two narrow lines and a broad resonance feature in the 200 to 0 ppm region. A representative ^{17}O spectra obtained from the one-pulse experiment at 8.45 T with a spinning rate of 14.6(±0.05) kHz is shown in Figure 3, with the two narrow lines shown in more detail in the inset. The two narrow lines were assigned to the two distinct Ti−O−Ti environments, and the broad feature was assigned to the eight similar Ti−O−P sites.

The shift in the position with field of the two narrow resonances was used to determine the quantity P_q according to the relationship

$$\delta_{\mathrm{obs}} = \delta_{\mathrm{iso}} - 6000\frac{P_q^{\,2}}{\nu_0^{\,2}} = \delta_{\mathrm{iso}} - 6000\frac{C_q^{\,2}\left(1 + \frac{\eta^2}{3}\right)}{\nu_0^{\,2}} \qquad (3)$$

C_q can be determined from the measured quantity P_q if η is independently known, which is not the case here. Because $0 \leq \eta \leq 1$, the value of C_q estimated from the P_q varies at most by 15%; therefore, P_q can be taken as a good estimate of the more fundamental quantity C_q. A linear fit to eq 3 using the measured chemical shifts at the three different field strengths resulted in the parameters assigned to the OT1 and OT2 sites given in Table 1.

Figure 4 shows the ^{17}O DOR spectrum at 16.95 T (upper) and 11.7 T (lower), in which the improved spectral resolution in the 200 to 0 ppm shift region is clearly visible. Analysis of the spectra reveals the presence of 10 isotropic lines, whereas only 8 lines are expected to correspond with the 8 distinct Ti−O−P sites. Assignments were made between corresponding lines in the spectra taken at the two different field strengths. The number of permutations in assigning the lines was reduced by (i) demanding that the δ_{obs} versus $1/\nu_0^2$ plot have a negative gradient for each site and (ii) requiring that the set of MAS lines generated from the DOR analysis provided acceptable agreement with experiment. Requirement (i) ruled out using any line from the 11.7 T data with a shift above 134 ppm (the highest

TABLE 1: Comparison of Measured and Calculated EFG Parameters for Different Atomic Sites in KTP[a]

site	$V_{zz}^{theoret}$ $\times 10^{21}$ V/m^2	$C_q^{theoret}$ MHz	$\eta^{theoret}$	$P_q^{theoret}$ MHz	C_q^{exptl} MHz	η^{exptl}	P_q^{exptl} MHz	δ_{cs}^{iso} ppm
K1	−2.44	3.45	0.58	3.84	3.6(1)	0.53(5)	3.9(1)	−45(±2)
K2	−2.24	3.17	0.26	3.24	3.1(1)	0.35(5)	3.2(1)	−75(±2)
OP1	8.14	5.03	0.18	5.08		∼0.2	3.6(5)	99(±10)
OP2	8.32	5.15	0.17	5.20		∼0.2	4.0(5)	100(±10)
OP3	8.50	5.26	0.27	5.39		∼0.2	4.4(5)	100(±10)
OP4	8.43	5.21	0.24	5.31		∼0.2	5.5(5)	150(±10)
OP5	8.49	5.25	0.20	5.32		∼0.2	4.7(5)	99(±10)
OP6	8.59	5.31	0.32	5.49		∼0.2	7.6(5)	128(±10)
OP7	8.38	5.18	0.22	5.26		∼0.2	4.4(5)	102(±10)
OP8	8.42	5.21	0.20	5.28		∼0.2	4.6(5)	100(±10)
OT1	1.26	0.78	0.92	1.00			1.1(5)	734(±5)
OT2	−2.03	1.26	0.41	1.33			1.8(5)	764(±5)
Ti(1)	−5.47	39.9	0.74	47.2	∼40			
Ti(2)	−6.24	45.6	0.30	47.0	∼40			

[a] The nuclear quadrupolar moments $Q(^{17}O) = 0.02558$ b, $Q(^{39}K) = 0.0585$ b, and $Q(^{47}Ti) = 0.302$ b have been assumed in obtaining the calculated parameters (see ref 24).

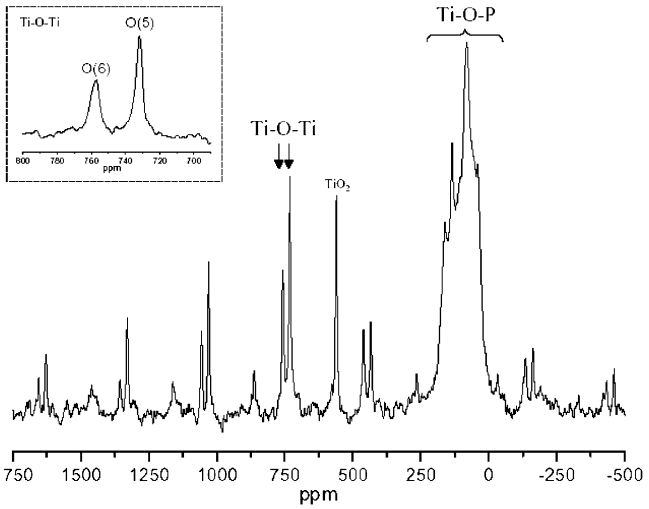

Figure 3. ^{17}O MAS NMR spectrum of KTP obtained at 8.45 T, with the bridging Ti−O−P sites and nonbridging Ti−O−Ti sites indicated together with the signal from a small amount of titania (anatase). The inset is a magnification of the narrow resonances assigned to the nonbridging OT1 and OT2 sites. The remaining unlabeled lines are spinning sidebands. The labels O(5) and O(6) on the inset refer to OT1 and OT2, respectively, assigned using the WIEN2k calculations as a guide.

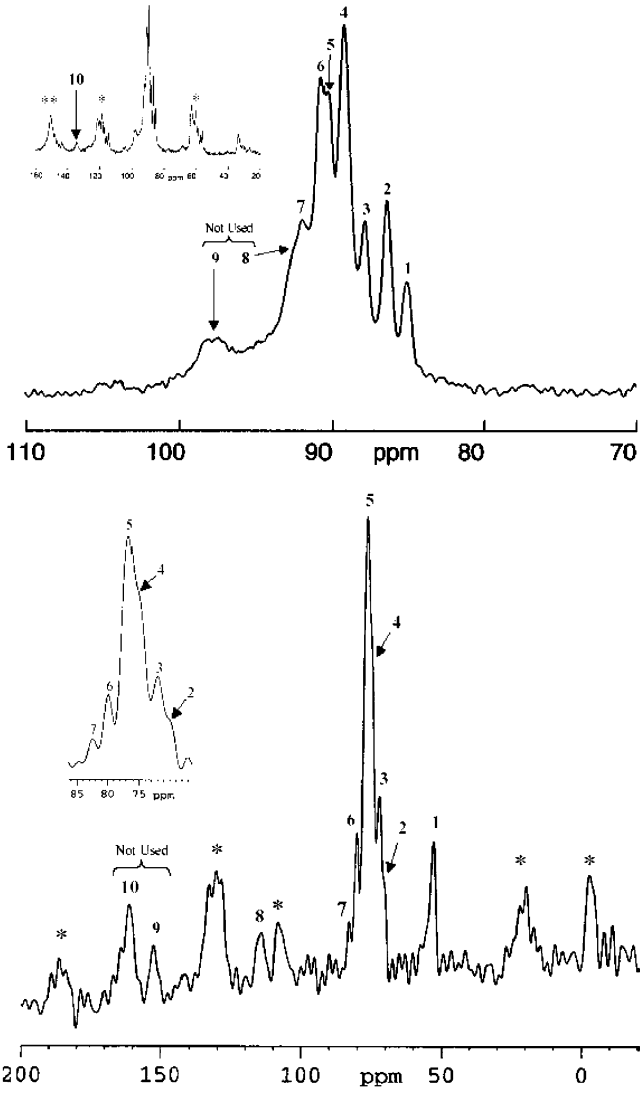

Figure 4. ^{17}O DOR spectra of KTP obtained at 16.95 T (top) and 11.7 T (bottom). Each isotropic line is numbered and the spinning sidebands are denoted by asterisks.

shift measured for the 16.95 T data) and immediately eliminated the lines at 151.5 and 160.5 ppm from the low-field data. Isotropic line positions and values of P_q were obtained from linear fits (Figure 5) to eq 1 and are given in Table 1. The parameters obtained were used together with $\eta = 0.2$ to simulate the MAS line shapes at different field strengths (Figure 6), for which the agreement between observed and calculated spectra is acceptable.

The presence of 10 rather than 8 isotropic lines in the DOR spectra remains unaccounted for. These extra lines are possibly due to a small amount of an ^{17}O-enriched second phase; however, none was detected by X-ray diffraction other than a small fraction of TiO_2 as indicated in Figure 3. The incomplete information used from the DOR spectra probably accounts for the deviation of the simulated from the observed MAS line shapes in Figure 6.

Titanium has two NMR active isotopes, ^{47}Ti and ^{49}Ti, with very similar, small gyromagnetic ratios but different spins and quadrupole moments giving lines whose width differs by a factor 3.45.[16] As mentioned earlier, the powder Ti spectrum (not shown) was unusually broad (∼2 MHz) and this, when combined with the low isotopic abundance and small gyromagnetic ratio, means that the signal was weak. The much larger width of the ^{47}Ti line means that this is the less intense of the

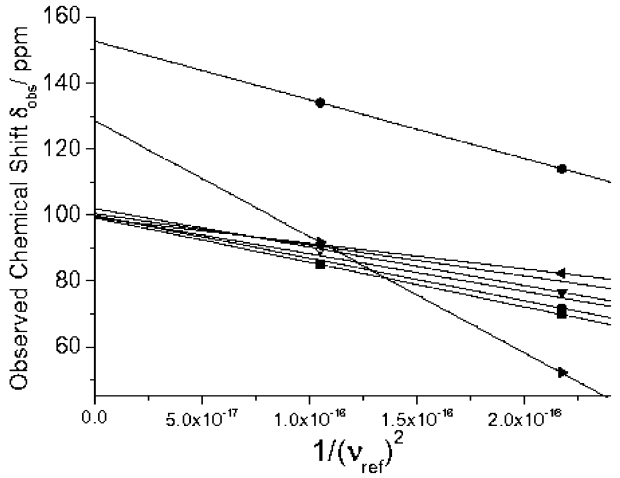

Figure 5. Plots of the observed chemical shift, δ_{obs}, as derived from the ^{17}O DOR data, vs $1/\nu_{ref}^2$ for the eight bridging Ti−O−P oxygens.

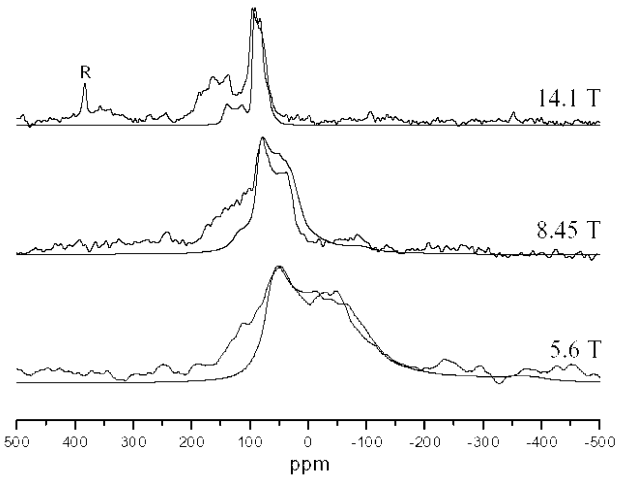

Figure 6. ^{17}O MAS NMR spectra of KTP in the 0 to 200 ppm chemical shift region showing the evolution of the broad feature assigned to the Ti−O−P sites as a function of field strength. R is a signal from the ZrO_2 rotor.

two, and therefore, we assume that the line width reported here is due to ^{49}Ti. The estimated C_q for this isotope is given in Table 1.

5. Discussion

5.1. Comparison between Experimentally Determined and Calculated NMR Parameters. Table 1 shows the comparison of the measured and calculated EFGs for the 2 independent K sites, Ti sites, and 10 independent O sites in the unit cell of KTP (Figure 1). The eight O's which are involved in bonds both to one of the P's and one of the Ti's are indicated as OP1−OP8, whereas the two O's that are bonded only to the Ti atoms and form the O−Ti−O−Ti chains of alternating long and short bonds are indicated by OT1 and OT2. The calculated C_q and η for the eight-coordinated K1 site are both within a few percent of the measured values for one K line, which was consequently assigned to the K1 site. The experimental C_q for the other line agrees well with that calculated for the K2 site, which also has a much smaller measured and calculated η. The $K1O_8$ site is invoked as having more importance for the nonlinear optical properties,[11] and the larger magnitude of C_q is in agreement with this.

The identification of the two OT sites was straightforward as two distinct sharp lines were evident with chemical shifts >730 ppm and giving P_q values consistent with the WIEN2k calculations for OT1 and OT2. The narrow line widths for the OT spectra indicate that the field gradients at the OT sites are considerably smaller than those at the OPs. According to the generally accepted[25−27] interpretation of NMR electric field gradients for ^{17}O, this implies that the OTs are more ionically bonded than the OPs. Consistent with this, the WIEN2k calculations show the OTs to have a more spherical electron density than that for the OPs. The larger EFGs at the OP sites are suggested to arise from the strong anisotropy produced by the covalent bonds in the PO_4 units. The bond-polarizability calculations of Xue and Zhang[11] suggest that the fractional covalencies of both the short and long Ti−OT contacts are smaller than those of the other Ti−OP bonds in agreement with the findings from NMR, as discussed in section 2.

The calculated P_q's for all of the OP sites lie in a narrow band of values between 5.08 and 5.49 MHz. The direction of the principal EFG axis is mainly determined by the direction of the short P−O bond. It is seen that the experimentally determined P_q values show a wider spread from 3.6(±0.5) MHz for OP1 to 7.6(±0.5) MHz for OP6 with five of the values being grouped in a narrow range of 4−4.7 MHz in closer agreement with the theoretical calculations. For all but OP3 and OP4, the WIEN2k calculations were used as a guide for assigning the NMR parameters to the different OPs. Contrary to the WIEN2k calculations, OP4 was assigned a higher measured P_q than O3 (note the WIEN2k P_q differs by only $\sim 1^1/_2$% for the two sites) because it computes to have a higher nonlinear susceptibility (see section 2). Although six of the eight OPs show chemical shifts in the range of 100(±2) ppm, the values for OP6 and OP4 are outliers. Detailed consideration of the local environment of OP6 shows that (i) it makes the shortest OP−P2 bond in the $P2O_4$ tetrahedron; (ii) it does not make a bonding contact to a potassium; (iii) it is the pivot atom in the largest Ti−OP−P linking angle of the structure (Ti1−OP6−P2 = 134.9°, compared with the mean value of 132.2 ± 2.2°); (iv) all other bond lengths and angles show a typical spread. By contrast, the environment of OP4 reveals no exceptional structural characteristics to explain the elevated chemical shift. The high field gradient at OP6 is consistent with a short P−O contact distance. If this were the only factor, then OP1, which makes the shortest P−O contact of all, should also have a similarly elevated field gradient. That it does not points to the additional importance of the Ti−O and K−O interactions, both of which are atypical for O1, in producing the local environment for each oxygen in the complex KTP structure.

5.2. Nonlinear Optical Properties of KTP: Comparison of NMR Results and Bond-Polarizability Theory. In bond-polarizability theory,[6] the fractional covalency, f_c, of a bond is given by the ratio

$$f_c = \left(\frac{E_h^\mu}{E_g^\mu}\right)^2 \tag{4}$$

where E_g^μ is the equivalent band gap for excitation of electrons in the μth bond between two species and E_h^μ is the homopolar (covalent) component of the gap. The band gap itself is given by the sum

$$(E_g^\mu)^2 = (E_h^\mu)^2 + (C^\mu)^2 \tag{5}$$

where C^μ is the heteropolar component of the gap. The nonlinear susceptibility

$$\chi^{\mu} = \frac{1}{4\pi}\left(\frac{\hbar\Omega_p^{\mu}}{E_g^{\mu}}\right)^2 \quad (6)$$

where Ω_p^{μ} is the plasma frequency for electrons in the bond, gives the nonlinear activity of the bonds of type μ. The final contribution to the crystal nonlinear susceptibility depends on the fraction of bonds of type μ and how they are arranged in the structure (geometrical conditions). The contributions of the different bonds are summed up tensorially to give the resultant nonlinear susceptibility.

The results of the NMR studies show a good correspondence with the most recently reported bond-polarizability calculations.[11] Figure 7a shows a plot of f_c for the Ti−O bonds versus the measured P_q's from NMR. It is seen that the Ti−OT bonds, both short and long, have fractional covalencies that are ≤50% of those of the other Ti−O bonds. This is consistent with the ^{17}O NMR results, which show the OTs with a distinct chemical shift and narrower lines, corresponding to a more ionic environment for these oxygens (fractional ionicity $f_i = 1 - f_c$).

The positive correlation (Figure 7a) between covalency and field gradient is important in independently validating the results of bond-polarizability calculations as the derivation of the f_c parameters, and the subsequent χ^{μ}'s for the bonds, is not ab initio and contains many approximations. Whereas the component E_h^{μ} of the band gap[6]

$$E_h^{\mu} = \frac{39.74}{(d^{\mu})^{2.48}} \quad (7)$$

where d^{μ} is the bond length (in Å) in question for E_h^{μ} (in esu), is a simple function of bond length and is easily calculated, the expression for C^{μ} is a more complex function of coordination number, effective charges, and bond length and contains parameters that must be obtained either by trial-and-error or by fitting to known optical constants. Because evaluation of C^{μ}, and thus E_g^{μ}, is not straightforward, the independent results of NMR, which corroborate the final estimates of f_c (and f_i) of the Ti−O bonds from the bond-polarizability theory, are important for establishing confidence in the use of this approach. It should be noted that the equivalent plot to Figure 7a using the theoretical P_q values obtained using WIEN2k does not show as smooth a correlation to f_c. Relative to the experimental values, the theoretical P_q's are too closely grouped in the range of 4−5 MHz and the value for O6 is grossly underestimated.

Plots of oxygen chemical shift against fractional covalency, gap energy, and so forth, typified by Figure 7b, do not reveal a smooth relationship. Rather, it is seen that the OPs all lie together on the left-hand side of the plot, with the chemical shift showing little variation with fractional covalency, whereas the OTs are in a separate area of parameter space. These plots confirm the radical divergence of chemical shift between the OTs and OPs, registering the very different resultant local environments that are seen by these two types of oxygen.

The simplified use of bond-polarizability theory applied in early discussions of the NLO properties of KTP assumed that the short Ti−OT bonds were the most covalent and accordingly assigned them high χ^{μ}'s. Because of the simple relationship between E_g^{μ} and bond length expressed in (7), it is true that the Ti−OT bonds have the largest absolute covalent component of the band gap. However, the more rapid increase of the heteropolar component C^{μ} as a function of decreasing bond length means that the fractional covalency of these bonds is finally smaller than that for any of the OPs. It should be noted that both short *and* long Ti−OT bonds compute to have the smallest f_c and χ^{μ} values of all the Ti−O bonds, although their geometrical disposition in the structure means that they are, nevertheless, the largest contributors to d_{333}, the component of the second-order nonlinear susceptibility directed along the polar axis. Ti2−OP6 and Ti1−OP4 are computed to have the most nonlinearly active bonds in agreement with the assignment of the largest field gradients and the outlying chemical shifts for these atoms.

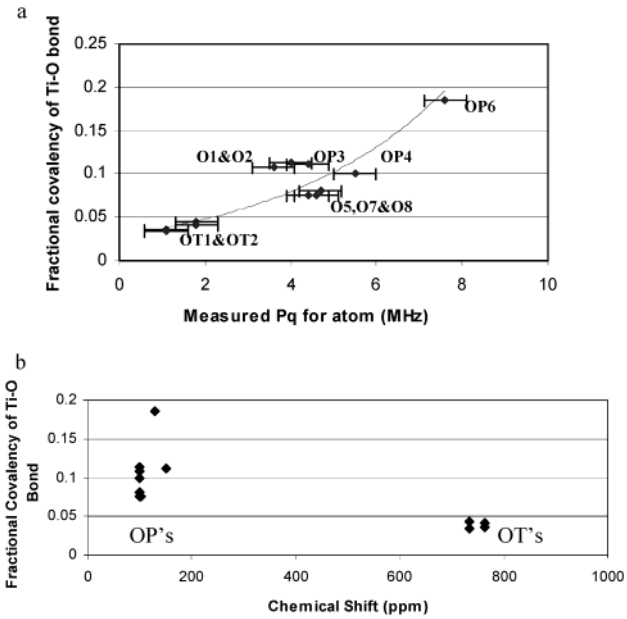

Figure 7. (a) Computed fractional covalencies (after Xue and Zhang[11]) of the 10 Ti−O bonds in the KTP structure vs the measured P_q parameters obtained from NMR experiments. The line is drawn as a guide to the eye. (b) Computed fractional covalencies vs chemical shift.

5.3. Comparison of NMR Parameters for Compounds Bearing Ti−O−Ti Chains. The EFGs at the OT1, OT2, and Ti sites in KTP are compared to those found for Ti−O−Ti sites in other titanates (Table 2). In titanite, $CaTiOSiO_4$, there exist chains of distorted octahedra, with alternating short (1.756(1) Å) and long (1.988(1) Å) Ti−OT bonds similar to those in KTP, although without the additional complication of the cis and trans orientations of the octahedra. The EFG at the OT site in $CaTiOSiO_4$ is only 0.2 MHz,[28] which is 20% or less of both the calculated and the experimental values for KTP.

$CaTiOSiO_4$ has structural similarities to KTP in that it incorporates both rigid tetrahedral units (SiO_4) and deformable octahedral (TiO_6) units in the structural framework. Similarly to KTP, the bridging Ti−O−Si oxygens show significantly broader resonances and larger EFGs than the OT species because of the covalent interactions in the SiO_4 groups. In contrast to KTP, the Ti EFG and the chemical shift of the OTs in titanite are both similar to the parameters for lead titanate, $PbTiO_3$, a perovskite structure that does not incorporate any framework building block other than the TiO_6 octahedron. These comparisons suggest that from the point of view of the oxygens, the OT−Ti−OT chains are essentially similar in character in $CaTiOSiO_4$ and $PbTiO_3$ with the OT environment being strongly ionic. We note, however, that there is a difference in the Ti environments in these two compounds since the EFG for Ti in $CaTiOSiO_4$ is 50% larger than the value in $PbTiO_3$ despite the octahedral distortion being only half as large. We can infer that there is a degree of covalency in the Ti−O interactions in titanite, imparted partly through the additional Ti−O−Si interactions, that does not exist in $PbTiO_3$.

TABLE 2: Comparison of EFG Parameters in Ti−O−Ti Chain-Bearing Materials[a]

formula and Ti coordination	short and long Ti−OT bonds (Å)	OT−Ti−OT angle in chain (deg)	octahedral distortion index (ref 30)	P_q's at OT site (MHz)	δ_{cs}^{iso} (ppm)	C_q at Ti site (MHz)
KTP (ref 7)	1.722	94.50	0.049(±0.005)	1.1(±0.5)	734(±5)	≈40
$Ti1O_6$	1.979					
KTP	1.744	174.9	0.040(±0.004)	1.8(±0.5)	765(±5)	≈40
$Ti2O_6$	2.095					
$CaTiOSiO_4$ (ref 31)	1.756	179.97	0.020(±0.002)	0.2 (ref 28)	632 (ref 28)	13.8(±0.2) (ref 30)
TiO_6	1.988					
$PbTiO_3$ (ref 32)	1.770	180	0.079(±0.005)	<0.5 (ref 34)	647(±5) (ref 34)	9.5(±0.1) (ref 30)
TiO_6	2.386					
$Li_2TiOSiO_4$ (ref 33)	1.697	179.98	not applicable		741 (ref 29)	13.2(±0.2) (ref 30)
TiO_5	(2.7015)[b]					

[a] TiO_6 indicates octahedral coordination and TiO_5 square pyramidal coordination. Errors in bond lengths are of the order of ±0.001 Å and those in angles are of the order of 0.04° (refer to the original structural papers, referenced in the first column of the table, for more specific information). [b] Not a bonding interaction but the distance to the more remote oxygen of the "chain".

The comparison between the ^{17}O and $^{47,49}Ti$ NMR spectra for KTP and the compound $Li_2TiOSiO_4$[29] is particularly striking. In $Li_2TiOSiO_4$, the Ti coordination environment is square pyramidal, with four equal Ti−O contacts (of length 1.967(1) Å) to the basal O1's and a short 1.698(1) Å contact to the apical O2. The O1 is used to link the TiO_5 units to the SiO_4 tetrahedra and is a Ti−O−Si bridging oxygen. The apical O2, however, makes no other primary contacts to the cations, because the Si's and Li's are both tetrahedrally coordinated only by O1's. TiO_5 pyramids can be considered to be linked into chains of alternating long and short Ti−OT bonds, which run along the [100] and [010] directions, if an exceptionally long Ti−O2 contact of 2.701 Å is included.

The ^{17}O NMR spectra for $Li_2TiOSiO_4$ show strong similarities with those for ^{17}O in KTP. In particular, there are two distinct ^{17}O signals: those for the bridging oxygens, which show a chemical shift of 157 ppm, and those identified with the nonbridging apical OTs, which show a chemical shift of 741 ppm. The latter chemical shift is very close to those observed for the OTs in KTP (Table 1). Furthermore, the spectra published by Bastow et al. also show that the line widths of the resonances of the apical O's are obviously narrower than those for the bridging O's in direct analogy to the behavior of the OPs and OTs in KTP.

5.4. Consequences for the KTP Structure. The comparisons between the compounds presented in Table 2 lead to the following proposals regarding the KTP structure:

(i) The large EFGs at the Ti sites should not be considered as arising from the local geometric distortion of the octahedral environment. Both experiment and WIEN2k calculations agree that these EFGs are far larger than should be expected from a local deformation model.

(ii) The OT environments in KTP should be seen as fundamentally different from those linking chains of similarly distorted octahedra in both $PbTiO_3$ and $CaTiOSiO_4$.

(iii) The OTs have a chemical shift consistent with isolated apical oxygens, suggesting that one Ti−OT interaction of each pair may be nonbonding.

In considering why the Ti−OT chains in KTP may differ from the other titanates, we start from a purely structural point of view and note that the principal geometrical difference between the chains of linked octahedra in KTP and the other examples in Table 2 is that $Ti1O_6$ and $Ti2O_6$ alternately adopt a cis and trans arrangement. This means that the equatorial planes of the two types of octahedra are perpendicular, being parallel to (010) and (100), respectively, for $Ti1O_6$ and $Ti2O_6$. The cis−trans arrangement necessitates the chain turning through an approximate right angle (OT1−Ti1−OT2 = 94.5-(1)°) at Ti1. By contrast, the chains for the other compounds listed in Table 2 are either close to or strictly linear (chain angles ≈180°). The right-angle turn in the KTP chain means that the center of the Ti1−OT2 short bond is only 2.9 Å from the center of the next Ti2−OT1 short bond in the chain. In the other compounds listed in Table 2 the equivalent distance ranges from 3.7 to 4.4 Å. The relatively close approach of the short-bond centers brought about by the 90° turn in KTP may provide a steric motivation for charge transfer out of the short-bonding region, both to distribute charge around the intermediate-length Ti−O bonds and to transfer significant charge density on to the long-bonded side of the OT atoms, as demonstrated in Figure 8, which is a contour map of the calculated (using WIEN2k) electron density around the Ti sites. For both types of TiO_6 octahedra, excess charge density is located on the long-bonded side of the Ti atom and the EFG of Ti points along the short-to-long bond direction (OT2−Ti1−OP1 or OT1−Ti2−OT2) for $Ti1O_6$ and $Ti2O_6$, respectively. Figure 8 suggests that there is bonding density in the long Ti−OT contacts for the calculated structure, although the long OT2−Ti2 contact is significantly weaker than the OT1−Ti1 interaction.

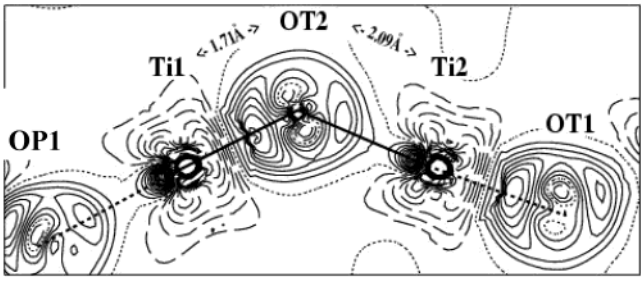

Figure 8. Theoretical difference electron density between crystal and superposed atoms in the plane containing Ti1−OT2−Ti2 (solid lines indicate the bonds). This structural feature appears at the right bottom corner of Figure 1. The other oxygens (OP1 and OT1) are not strictly in the same plane but close to it (bonds are indicated by dashed lines). Note that the short Ti1−OT2 bond is opposite the long Ti1−OP1 bond, whereas in the Ti2O6 octahedron, the short Ti2−OT1 bond lies opposite the long Ti2−OT2 bond (distances indicated by arrows).

The anomalously high field gradients at the Ti's and the unusual properties of the OTs suggest that there may be complex charge-transfer mechanisms occurring in the KTP structure. Jarman et al.[35] have previously put forward a "conjugated" chain notion of KTP. From closed-shell Hartree−Fock calculations on a model KTP-like system, they concluded that the more distant OTs in the Ti−OT−Ti chains do *not* make bonding interactions and noted that "titanium apparently acts as a conduit through which electron density is shifted... with the total shift

proportionally greater than the geometric distortion". The latter property of Ti as the "conduit" for charge transfer is consistent with the highly elevated EFG over and above the value expected from local octahedral distortions. The findings from NMR also support Jarman et al.'s assertion that the long Ti−OT contacts are nonbonding, via the similarity between the chemical shifts of the OTs in KTP and $Li_2TiOSiO_4$, but the WIEN2k calculations (Figure 8) presently contradict this conclusion. Streltsov et al.[12] have also suggested that charge-transfer processes, producing pronounced electron density depletion and excess waves, take place in TiO_6-AsO_4 chains of $RbTiOAsO_4$, which may further act to enhance the EFG at the Ti sites and certain of the OP sites, such as OP6, in KTP-like compounds.

6. Concluding Remarks

The findings of this NMR study regarding the covalent/ionic character of the OT and OP interactions agree with the semiempirical bond-polarizability theory as applied by Xue and Zhang.[11] In their work, the large optical nonlinearity of KTP is mainly attributed to the PO_4 and KO_8/KO_9 groups with the bond-polarizabilities in the Ti−O groups making small contributions overall. Despite this, it is certainly true that when the octahedral distortions are reduced by, for example, substituting Ti by Ge or Sn, the nonlinear activity of the resultant material reduces sharply compared with KTP itself. Therefore, the presence of Ti in a highly distorted octahedral environment is necessary, although not sufficient, for high optical nonlinearity to be displayed.

The anomalously high electric field gradients at the Ti sites, which cannot be accounted for by the local octahedral distortions, suggest that models for the nonlinear optical properties of KTP that rely principally on measures of distortion at the Ti sites will fail for similar reasons, that is, that the origin of the high asymmetry at this site is other than geometric. The large EFGs at the Ti sites and associated charge-transfer mechanisms are suggested to be important factors in establishing the necessary conditions for a high nonlinear response.

Acknowledgment. A. Baldwin thanks EPSRC for funding a Ph.D. studentship. The NMR equipment used for this study was partly funded by the Engineering and Physical Sciences Research Council and the National High Magnetic Field Laboratory.

References and Notes

(1) Zumsteg, F. C.; Bierlein, J. D.; Gier, T. E. *J. Appl. Phys.* **1976**, *47*, 4980.
(2) Chani, V. I.; Shimamura, K.; Yu, Y. M.; Fukuda, T. *Mater. Sci. Eng.* **1997**, *R20*, 281.
(3) Stucky, G. D.; Phillips, M. L.; Gier, T. E. *Chem. Mater.* **1989**, *1*, 492.
(4) Hansen, N. K.; Protas, J.; Marnier, G. *C. R. Acad. Sci.* **1988**, *307*, 475.
(5) Thomas, P. A.; Glazer, A. M.; Watts, B. E. *Acta Crystallogr., Sect. B* **1990**, *46*, 333.
(6) Levine, B. F. *Phys. Rev. B* **1973**, *7*, 2600.
(7) Hansen, N. K.; Protas, J.; Marnier, G. *Acta Crystallogr., Sect. B* **1991**, *47*, 660.
(8) Phillips, M. L. F.; Harrison, W. T. A.; Stucky, G. D.; McCarron, E. M.; Calabrese, J. C.; Gier, T. E. *Chem. Mater.* **1992**, *4*, 222.
(9) Harrison, W. T. A.; Phillips, M. L. F.; Stucky, G. D. *Chem. Mater.* **1997**, *9*, 1138.
(10) Mayo, S. C.; Thomas, P. A.; Teat, S. J.; Loiacono, G. M.; Loiacono, D. *Acta Crystallogr., Sect. B* **1994**, *50*, 655.
(11) Xue, D.; Zhang, S. *J. Solid State Chem.* **1999**, *142*, 156.
(12) Streltsov, V. A.; Nordborg, J.; Albertsson, J. *Acta Crystallogr., Sect. B* **2000**, *56*, 785.
(13) Han, J. K.; Oh, D. K.; Lee, C. H.; Lee, C. E.; Kim, J. N.; Kim, S. C. *Phys. Rev. B* **1997**, *55*, 2687.
(14) Kim, K. S.; Park, E. R.; Lee, C. H.; Oh, D. K.; Lee, C. E.; Dalal, N. S.; Fu, R. *Phys. Rev. B* **2001**, *64*, 132409.
(15) Crennell, S. J.; Owen, J. J.; Grey, C. P.; Cheetham, A. K. *J. Mater. Chem.* **1992**, *2*, 785.
(16) Padro, D.; Howes, A. P.; Smith, M. E.; Dupree, R. *Solid State Nucl. Magn. Reson.* **2000**, *15*, 231.
(17) Perdew, J.; Burke, S.; Ernzerhof, M. *Phys. Rev. Lett.* **1996**, *77*, 3865.
(18) Madsen, G. K. H.; Blaha, P.; Schwarz, K.; Sjöstedt, E.; Nordström, L. *Phys. Rev. B* **2001**, *64*, 195134.
(19) Blaha, P.; Schwarz, K.; Madsen, G. K. H.; Kvasnicka, D.; Luitz, J. *WIEN2k, An Augmented Plane Wave + Local Orbitals Program for Calculating Crystal Properties*; Technische Universität Wien: Austria, 2001; ISBN 3-9501031-1-2.
(20) Delarue, P.; Lecomte, C. Department of Crystallography and Minerology, University of Nancy, France. Private communication, 2003.
(21) Schwarz, K.; Blaha, P. *Z. Naturforsch.* **1992**, *47A*, 197.
(22) Dufek, P.; Blaha, P.; Schwarz, K. *Phys. Rev. Lett.* **1995**, *75*, 3545.
(23) Blaha, P.; Schwarz, K.; Faber, W.; Luitz, J. *Hyperfine Interact.* **2000**, *126*, 389.
(24) Pyykkö, P. *Mol. Phys.* **2001**, *99*, 1617.
(25) Samoson, A.; Lippmaa, E. *J. Magn. Reson.* **1989**, *84*, 410
(26) Schramm, S.; Oldfield, E. *J. Am. Chem. Soc.* **1984**, *106*, 2502.
(27) Oldfield, E.; Coretsopoulos, C.; Yang S.; Reven, L.; Lee, H. C.; Shore, J.; Han, O. H.; Ramli, E.; Hinks, D. *Phys. Rev. B* **1989**, *40*, 6832−6845.
(28) Kroeker, S.; Rice, D.; Stebbins, J. F. *Am. Mineral.* **2002**, *87*, 572.
(29) Bastow, T. J.; Moodie, A. F.; Smith, M. E.; Whitfield, H. J. *Acta Crystallogr., Sect. A* **1999**, *55*, 127.
(30) Padro, D.; Jennings, V.; Smith, M. E.; Hoppe, R.; Thomas, P. A.; Dupree, R. *J. Phys. Chem. B* **2002**, *106*, 13176.
(31) Kek, S.; Arroyo, M.; Bismayer, U.; Schmidt, C.; Eichhorn, K.; Krane, H. G. *Z. Kristallogr.* **1997**, *212*, 9.
(32) Nelmes, R. J.; Kuhs, W. F. *Solid State Commun.* **1985**, *54*, 721.
(33) Ziadi, A.; Thiele, G.; Elouadi, B. *J. Solid State Chem.* **1994**, *109*, 112.
(34) Baldwin, A. Ph.D. Thesis, University of Warwick, 2003.
(35) Jarman, R. H.; Munowitz, M.; Harrison, J. F. *J. Cryst. Growth* **1991**, *109*, 353.